Multi-Light-Responsive Quantum Dot Sensitized Hybrid Micromotors with Dual-Mode Propulsion

Roberto Maria Hormigos, Beatriz Jurado S#nchez, and Alberto Escarpa**

Abstract: CdS quantum dots/C_{60} tubular micromotors with chemical/multi-light-controlled propulsion and "on-the-fly" acceleration capabilities are described. In situ growth of CdS quantum dots on the outer fullerene layer imparts this layer with light-responsive properties in connection to inner Pt, Pd or MnO_2 layers. This is the first time that visible light is used to drive bubble-propelled tubular micromotors. The micromotors exhibit a broad absorption range from 320 to 670 nm and can be wirelessly controlled by modulating light intensity and peroxide concentration. The built-in accelerating optical system allows for the control of the velocity over the entire UV/Vis light spectra by modulating the catalyst surface chemistry. The light-responsive properties have been also exploited to accelerate the chemical dealloying and propulsion of micromotors containing a Cu/Pd layer. Such dual operated hybrid micromotors hold considerable promise for designing smart micromachines for on-demand operations, motion- based sensing, and enhanced cargo transportation.

Natural protein motors[1] have inspired scientist to create artificial micromotors powered by bubble thrust, diffusiophoresis,[2] or self-electrophoresis mechanisms.[3] Such moving objects have opened new possibilities in the biomedical,[4] environmental,[5] and analytical fields.[6] Yet, directional control is essential to perform "on-demand" tasks. To date, this has been achieved by the application of external magnetic fields,[7] light[8] or using topographical pathways.[9] Light is a versatile physical external stimulant to tailor the propulsion of self-propelled micromotors[10] in connection with photocatalytic materials. TiO_2[11] and TIO_2/Au nanowires,[12] TiO_2/Pt,[13] TiO_2/Au,[14] WO_3,[15] and α-Fe_2O_3[16] Janus micromotors exhibit enhanced propulsion in water or peroxide solutions by a UV-light-induced phoretic mechanism. Interestingly, the Wang group described TiO_2 micromotors decorated with Au nanoparticles with a built-in optical braking system.[13a] Yet, the harmful effect of UV light to living organisms stimulated the design of visible-light-propelled micromotors such as Cu_2O/Au,[17] bismuth oxyiodide,[18] TiO_2/Cu_2O,[19] and TiO_2/Mo_7/Au[20] Janus micromotors. Panne et al. coated black TiO_2 spheres with an Au layer for efficient light-induced propulsion over the entire UV/Vis light spectra and "ON-OFF-ON" motion behavior.[21] More interestingly, near-infrared (NIR) light has been exploited for micromotor propulsion and drug-triggered release schemes, holding considerable promise for practical biomedical applications in the near future.[22] ZnO/Pt[23] and TiO_2[14,24] bubble-propelled tubular micromotors exhibit highly enhanced propulsion (accelerating systems) upon UV-light illumination due to enhanced fuel decomposition, reaching speeds of up to 600 *m*m $s^{@1}$.[23] Despite the progress achieved so far in the use of light to control the direction and speed of micromotors, limitations still exist that require more research. For example, the relatively low speeds of self-electrophoretic micromotors, which range from 5 to 40 *m*m $s^{@1}$,[10] limit the practical application in real settings where the presence of, for example, salts and proteins can deactivate them. Further- more, the fabrication process entails complex and expensive preparation procedures, such as electron-vapor deposition and requires noble metals, such as Au of Pt.[10] The aim of this paper is to fill some of the aforementioned gaps in light- driven micromachines namely, efficient propulsion, multi- light motion control, and cost-effective preparation.

Herein, we describe the preparation of CdS quantum dots/ C_{60} tubular micromotors based on different catalyst (Pt, Pd, and MnO_2) and its "on-demand" accelerating behavior upon irradiation with UV, visible, or IR light. Photocatalytic materials, such as quantum dots, can be generated in situ during the electrodeposition of the first outer layer.[25] This results into a light-responsive matrix, to achieve wirelessly controlled and light-enhanced propulsion by the real-time tailoring of chemical reactions on the inner catalytic surface. Upon light irradiation (at 385 to 670 nm), electrons present in the valence band in the CdS quantum dots migrate to the conduction band, creating an electron–hole pair. Such electrons are then trapped in the Pt or Pd catalytic layers, resulting in a negative net charge in the metal size, which reacts with oxygen and protons present in the media, generating further H_2O_2 input, which is further decomposed and increases the overall micromotor speed. When using MnO_2 as catalytic layer, such electrons recombine with its electronic levels, and migrate to the conduction band, creating holes (h^+) which also react with H_2O_2 fuel, generating more O_2 and leading to a dramatic enhanced micromotor acceleration (Figure 1). Such velocity can be modulated by adjusting the light intensity and fuel concentration. We will also illustrate the effect of light on the acceleration of the dealloying of an inner catalytic Cu/Pd layer.

Figure 1 illustrates the dual chemical- and light-driven propulsion of the micromotors. The multi-light responsive hybrid micromotors were synthetized by a modified template electrodeposition protocol.[26] For more details of micromotor synthesis and characterization,[26] see Figures S1–S3 in the Supporting Information. An optical acceleration system has been achieved by using visible or UV light to enhance the catalytic reaction (ON). Such motion studies were examined by optical microscopy using UV- and visible-light sources, coming directly from the objectives (see Experimental Section for more details). Upon UV- or visible-light irradiation, CdS quantum dots on the micromotor surface absorb photons with energies equal to or higher than its bang gap energy (2.2 eV). Different light illuminations along the spectra were used, which correspond to variable photon energies: 385 (3.2 eV), 470 (2.6 eV), 550 (2.3 eV), and 670 nm (1.9 eV). Such electrons are then trapped in the catalytic layers, resulting in a negative net charge in the metal size, which reacts with oxygen and protons present in the media, generating additional H_2O_2 input. In the absence of light (OFF) the lack of additional H_2O_2 input results in a decrease in the speed.

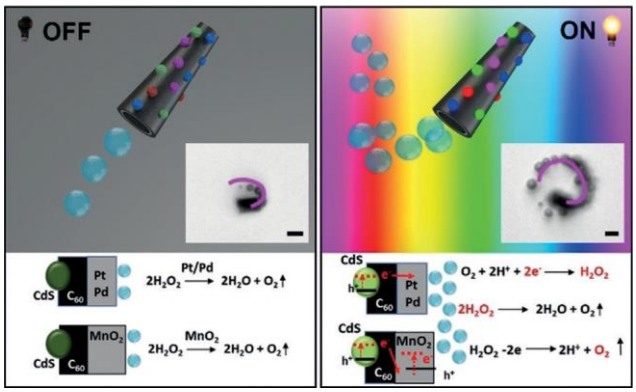

Figure 1. Schematic and time-lapse images of the propulsion of CdS/C_{60} micromotors based on Pd, Pt, or MnO_2 catalysts without (OFF) and with (ON) UV- or visible-light illumination and related propulsion mechanisms (the in situ H_2O_2 or O_2 generated by light illumination is shown in red). Inset shows tracking lines of the micromotor moving in 5% peroxide solutions at each condition. Scale bars, 5 *m*m.

The time-lapse images and trajectories of Figure 2a clearly illustrate the enhanced micromotor propulsion upon light illumination. Thus, the initial speed of Pt micromotors before light irradiation (670 ± 61 μm s-1) increased to 950 ± 70, 1058 ± 72 and 870 ± 60 μm s^{-1} after exposure to UV (385 nm), blue (470 nm), and green (550 nm) visible light, respectively. As expected, no apparent changes in the initial speed were noted after irradiation with red light (670 nm) because the band gap (1.9 eV) is lower than the bandgap of the CdS quantum dots, preventing photon absorption and electron promotion. Such a speed increase (up to 1.5 times) is attributed to the migration of electrons present in the valence band in the CdS quantum dots to the conduction band, creating an electron–hole pair. The C_{60} supporting layer also acts as electron acceptor,[27] promoting electron transport towards the Pt layer. Once in the metallic/catalytic layer, electrons accumulate, resulting in a negative net charge that reacts with oxygen and protons present in the media, generating additional H_2O_2 input, which is further decomposed and increases the micromotor speed.[23] A similar behavior was observed when using the noble metal Pd. The speed increased from 70 ±10 to 145 ± 20 (UV), 105 ± 15 (blue), and 99 ± 12 μm s^{-1} (green), with no apparent changes after illumination with red light. Such enhanced movement (up to two times) is also reflected in the trajectories of Figure 2a and the corresponding movies found in the Supporting Information. A more dramatic speed enhancement over the entire spectra was noted when using MnO_2. Such a catalyst is a cost-effective alternative to noble metals for the mass-scale preparation of micromotors. In this case, the speed increased up to 1.6 times after irradiation with the different lights, from 148 ± 20 to 211 ± 27 μm s^{-1} (violet to green). As MnO_2 possess a photocatalytic-like behavior,[28] electrons from the CdS/C_{60} layer recombine with the MnO_2 electronic levels, and migrate to the conduction band, creating holes (h^+) which also reacts with H_2O_2 fuel, generating additional O_2 and leading to a dramatic enhanced micromotor acceleration, similar to TiO_2.[29] Hydrogen peroxide generation was monitored by chronoamperometry. To this end, a 10 *m*L drop of CdS/C_{60}-Pt or CdS/C_{60}-MnO_2 micromotors was placed on a glass slide and irradiated with light (470 nm) for 5 min.

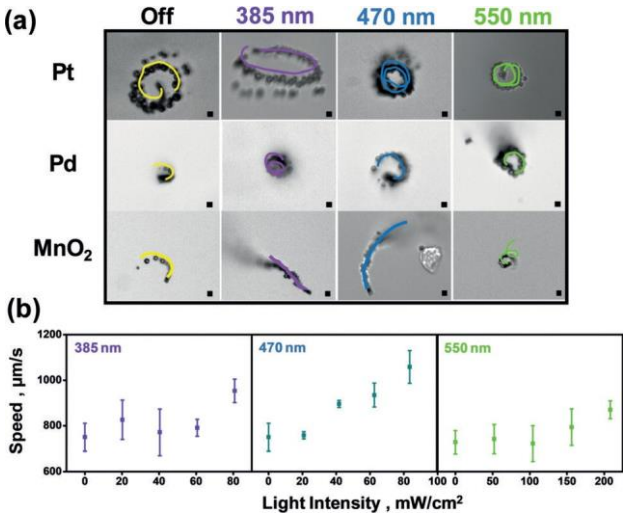

Figure 2. Effect of UV- and visible-light intensity on the propulsion of CdS/C_{60} micromotors based on Pd, Pt, or MnO_2 catalysts. (a) Time-lapse images (Taken from Videos S1–S3 in the Supporting Information) of the micromotor propulsion in 5% peroxide solutions and (b) Dependence of speed on different light intensities. Scale bars, 5 *m*m.

Control experiments using C_{60}-Pt or C_{60}-MnO_2 micromotors were also performed. After irradiation, drops were placed on a Pt screen printed electrode containing PBS buffer with an applied potential of 0.70 V. As can be seen in Figure S4 in the Supporting Information, a drastic increase in the chronoamperometric response was noted after addition of the CdS/C_{60}-MnO_2 drop, which was attributed to the gener- ation of hydrogen peroxide due to light irradiation and the effect of the CdS quantum dots. No signal increase was noted when using control micromotors. Similar results were obtained when using Pt or Pd as catalyst. Such a current increase further supports the proposed mechanism. To further support the role of CdS quantum dots for micromotor propulsion, control experiments were performed with C_{60}-Pt, C_{60}-MnO_2, PEDOT-Pt, and PEDOT-MnO_2 micromotors with the different lights used. As can be seen in Figure S5 in the Supporting Information, no obvious speed increase was noted before or after irradiation of the control micromotors with the different lights. Such results corroborate the crucial and sole role of the CdS quantum dots in the speed enhancement due to its photocatalytic nature. Furthermore, the possible heat effect caused by light irradiation does not have any apparent influence on speed.

The speed of the micromotors can be also modulated by incident light intensity, according to Equation (1):[21,23]

$$I = \emptyset\ h\ c/\ \lambda \qquad (1)$$

where $\emptyset$, *h*, *c*, and λ are the incident photon flux, Planck constant, speed of light, and wavelength of incident light, respectively. Figure 2b illustrates that the speed can be modulated by different light intensities (at a fixed peroxide concentration of 5 %) at each wavelength, with an increase in the velocity along with the intensity. This trend is more remarkable at 470 nm. Please note here that this data corresponds to Pt micromotor, but the same trend was observed for Pd and MnO_2 micromotors.

The combined effect of light intensity, light wavelength, and peroxide concentration on the micromotor propulsion and speed is shown in the plots in Figure 3. Incident photon flux (∅), calculated according to Equation (1), was $2.6 \times 10^{@3}$, $3.2 \times 10^{@3}$, $9.5 \times 10^{@3}$, and $4.1 \times 10^{@3}$ molm$^{@2}$ s$^{@1}$ for UV, cyan, green, and red light, respectively. Micromotor speed increased along with the H_2O_2 concentration, but decreased as the wavelength increased (except at 670 nm, where the incident light does not directly interact with the CdS quantum dots). This is due to a decrease in light absorption with increasing wavelength, as reflected in the UV spectra of Figure S1 in the Supporting Information and the band gap of CdS quantum dots (2.2 eV). Thus, fewer electron–hole pairs are produced and the peroxide decomposition decreases. Please note that such differences arise from the different wavelength intensities used, which are imposed by the experimental settings. The intensities for 365, 470, 550, and 760 nm light illuminations are 808, 835, 2083, and 749 W m^{-1}, respectively. As results in Figure 3b are expressed as speed/photon flux, the highest photon flux (associated with the high intensity) at 550 nm results in a dramatic reduction in this relationship. Next, at 670 nm, there is a decrease in the photon flux, resulting in an increase in the relation speed/photon flux. Such fact can be exploited for the "on-demand" braking/acceleration of these micromotors for a myriad of applications as an alternative to magnetic control and in motion-based detection schemes.

To further prove the concept of the use of light to activate micromotors, the effect of different light irradiations on the controlled chemical activation (via Cu corrosion) of micromotors with a Cu/Pd inner layer was studied. Activation time can be tailored by controlling the composition of the surrounding media (for example fuel, NaCl concentration, and local pH),[30] but this is the first time that light has been evaluated as potential trigger for such controlled propulsion. At acidic conditions (pH 3.5 in this work), peroxide can dissolve/corrode copper via electron-transfer, as follows [Eqs. (2)–(3)]:[30,31]

$$2Cu \leftrightarrows 2Cu^{+} + 2\,e^{-} \quad (2)$$

$$H_2O_2 + 2H^{+} + 2e^{-} \leftrightarrows 2H_2O \quad (3)$$

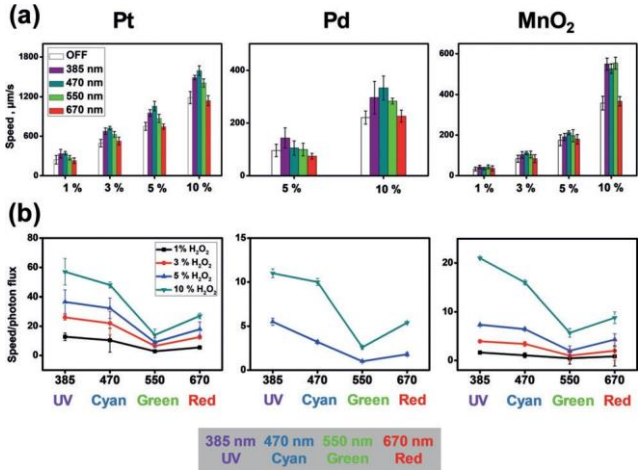

Figure 3. (a) Effect of peroxide concentration on the speed of CdS/C_{60} micromotors based on Pt, Pd or MnO_2 catalysts under UV and four different visible light illuminations. (b) Speed/photon flux as a function of wavelength at different H_2O_2 concentrations.

One surprising fact is that after Cu dissolution and ignition, the speed of the micromotors increases after irradiation with red light (670 nm), which can be attributed to the generation of Cu_xS quantum dots in the micromotor surface via cationic exchange of Cu^{+} and related ions in solution, as previously described.[32,33] The band gap of CuS and $Cu_{1.8}S$ quantum dots is 1.2 and 1.5 eV, respectively.[34] This decrease in the band gap is lower than the photon energy of the incident light (1.9 eV), thus initiating electron transfer and enhanced peroxide production at increased speeds. Another hypothesis here was that, due to light illumination, the electrons irradiated by the CdS quantum dots will interact with the gradually exposed Pd layer, generating additional H_2O_2 and accelerating the dealloying effect, reducing the activation time. Surprisingly, as can be seen in Figure 4 b, no apparent effect was noted after irradiation with light at 385 and 470 nm, as the micromotors started to propel after 10 min addition of the peroxide fuel (which was also observed in the absence of light). This can be due the low level of Pd surface exposed after Cu dissolution, which prevents the enhanced peroxide production effect. Yet, for 550 and 670 nm light, micromotors started to propel after 8 and 5 min peroxide addition, respectively (see also Video S4 in the Supporting Information), probably due to an acceleration in the kinetics of the aforementioned reaction.[32]

In conclusion, we have described CdS-quantum-dots-sensitized C_{60} tubular micromotors with a built-in optical acceleration system. Such dual operated hybrid micromotors hold considerable promise for designing smart micromachines that autonomously reconfigure their propulsion mode for on-demand operations, motion-based sensing, and enhanced cargo transportation.

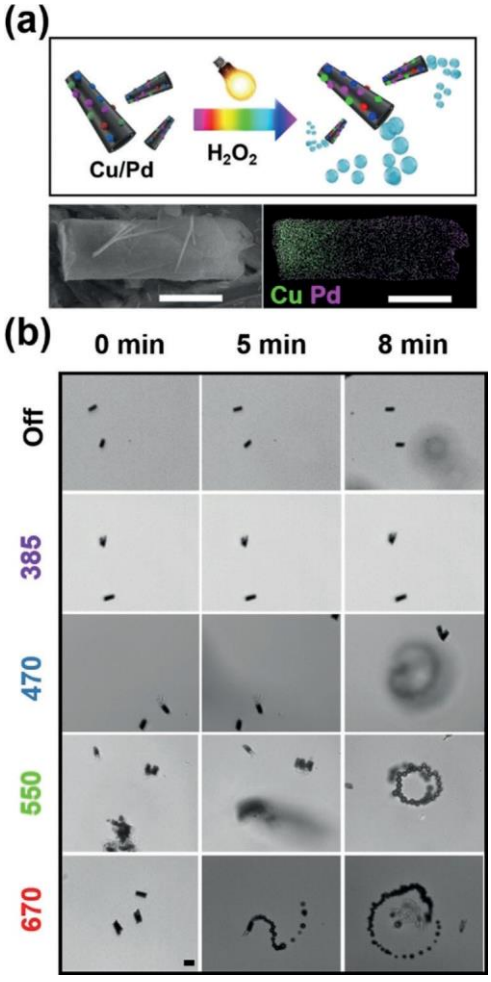

Figure 4. UV- and visible-light controlled chemical activation of CdS/C_{60} micromotors with an inner Cu/Pd alloy layer. (a) Illustration of the controlled propulsion mechanism. SEM and EDX images of the micromotors. (b) Time-lapse images of the micromotors without and with UV- and visible-light illumination in 1 % H_2O_2 solutions. Scale bars, 5 *m*m.

Acknowledgements

Spanish Ministry of Economy and Competitiveness (BES-2015-072346, RYC-2015-17558, co-financed by EU and CTQ2017-86441-C2-1-R. Community of Madrid. (S2013/MIT-3029).

Conflict of interest

The authors declare no conflict of interest.

Keywords: light · micromotor · nanomotor · propulsion · quantum dot

References

[1] H. Peng, X. F. Li, H. Zhang, X. C. Le, *Nat. Commun.* 2017, *8*, 14378.

[2] a) W. F. Paxton, K. C. Kistler, C. C. Olmeda, A. Sen, S. K. St. Angelo, Y. Cao, T. E. Mallouk, P. E. Lammert, V. H. Crespi, *J. Am. Chem. Soc.* 2004, *126*, 13424 – 13431; b) G. A. Ozin, I. Manners, S. Fournier-Bidoz, A. Arsenault, *Adv. Mater.* 2005, *17*, 3011 – 3018; c) W. F. Paxton, S. Sundarajan, T. E. Mallouk, A. Sen, *Angew. Chem. Int. Ed.* 2006, *45*, 5420 – 5429; *Angew. Chem.* 2006, *118*, 5546 – 5556; d) A. A. Solovev, Y. Mei, E. Bermfflde- z UreÇa, G. Huang, O. G. Schmidt, *Small* 2009, *5*, 1688 – 1692; e) S. J. Ebbens, J. R. Howse, *Soft Matter* 2010, *6*, 726; f) J. Wang, *Nanomachines: Fundamentals and Applications*, Wiley-VCH, Weinheim, 2013; g) W. Gao, S. Sattayasamitsathit, J. Orozco, J. Wang, *J. Am. Chem. Soc.* 2011, *133*, 11862 – 11864.

[3] W. Wang, T. Y. Chiang, D. Velegol, T. E. Mallouk, *J. Am. Chem. Soc.* 2013, *135*, 10557 – 10565.

[4] a) B. Esteban-Fern#ndez de _vila, W. Gao, E. Karshalev, L. Zhang, J. Wang, *Acc. Chem. Res.* 2018, *51*, 1901 – 1910; b) F. Peng, Y. Tu, D. A. Wilson, *Chem. Soc. Rev.* 2017, *46*, 5289 – 5310.

[5] B. Jurado-S#nchez, J. Wang, *Environ. Sci. Nano* 2018, *5*, 1530 – 1544.

[6] L. Kong, J. Guan, M. Pumera, *Curr. Opin. Electrochem.* 2018, *10*, 174 – 182.

[7] R. Maria-Hormigos, B. Jurado-S#nchez, A. Escarpa, *Nanoscale* 2017, *9*, 6286 – 6290.

[8] A. A. Solovev, E. J. Smith, C. C. Bof' Bufon, S. Sanchez, O. G. Schmidt, *Angew. Chem. Int. Ed.* 2011, *50*, 10875 – 10878; *Angew. Chem.* 2011, *123*, 11067 – 11070. F.a) J. Simmchen, J. Katuri, W. E. Uspal, M. N. Popescu, M. Tasinkevych, S. Sánchez, *Nat. Commun.* 2016, *7*, 10598; b) X. Lu, F. Soto, J. Li, T. Li, Y. Liang, J. Wang, *ACS Appl. Mater. Interfaces* 2017, *9*, 38870 – 38876.

[9] R. Dong, Y. Cai, Y. Yang, W. Gao, B. Ren, *Acc. Chem. Res.* 2018, *51*, 1940 – 1947.

[10] C. Chen, F. Mou, L. Xu, S. Wang, J. Guan, Z. Feng, Q. Wang, L. Kong, W. Li, J. Wang, Q. Zhang, *Adv. Mater.* 2017, *29*, 1603374.

[11] B. Dai, J. Wang, Z. Xiong, X. Zhan, W. Dai, C.-C. Li, S.-P. Feng, J. Tang, *Nat. Nanotechnol.* 2016, *11*, 1087.

[12] a) C. Chen, S. Tang, H. Teymourian, E. Karshalev, F. Zhang, J. Li, F. Mou, Y. Liang, J. Guan, J. Wang, *Angew. Chem. Int. Ed.* 2018, *57*, 8110 – 8114; *Angew. Chem.* 2018, *130*, 8242 – 8246; b) F. Mou, L. Kong, C. Chen, Z. Chen, L. Xu, J. Guan, *Nanoscale* 2016, *8*, 4976 – 4983; c) L. Kong, C. C. Mayorga-Martinez, J. Guan, M. Pumera, *ACS Appl. Mater. Interfaces* 2018, *10*, 22427 – 22434.

[13] R. Dong, Q. Zhang, W. Gao, A. Pei, B. Ren, *ACS Nano* 2016, *10*, 839 – 844.

[14] Q. Zhang, R. Dong, Y. Wu, W. Gao, Z. He, B. Ren, *ACS Appl. Mater. Interfaces* 2017, *9*, 4674 – 4683.

[15] a) J. Palacci, S. Sacanna, A. Abramian, J. Barral, K. Hanson, A. Y. Grosberg, D. J. Pine, P. M. Chaikin, *Sci. Adv.* 2015, *1*, e1400214; b) J. Palacci, S. Sacanna, A. P. Steinberg, D. J. Pine, P. M. Chaikin, *Science* 2013, *339*, 936 – 940.

[16] D. Zhou, Y. C. Li, P. Xu, N. S. McCool, L. Li, W. Wang, T. E. Mallouk, *Nanoscale* 2017, *9*, 75 – 78.

[17] R. Dong, Y. Hu, Y. Wu, W. Gao, B. Ren, Q. Wang, Y. Cai, *J. Am. Chem. Soc.* 2017, *139*, 1722 – 1725.

[18] a) E. O'Neel-Judy, D. Nicholls, J. Castaneda, J. G. Gibbs, *Small* 2018, *14*, e1801860; b) L. Wang, M. N. Popescu, F. Stavale, A. Ali, T. Gemming, J. Simmchen, *Soft Matter* 2018, *14*, 6969 – 6973.

[20] A. Mallick, S. Roy, *Nanoscale* 2018, *10*, 12713 – 12722.

[21] B. Jang, A. Hong, H. E. Kang, C. Alcantara, S. Charreyron, F. Mushtaq, E. Pellicer, R. Buchel, J. Sort, S. S. Lee, B. J. Nelson, S. Pane, *ACS Nano* 2017, *11*, 6146 – 6154.

[22] a) Z. Wu, X. Lin, Y. Wu, T. Si, J. Sun, Q. He, *ACS Nano* 2014, *8*, 6097 – 6105; b) Z. Wu, X. Lin, X. Zou, J. Sun, Q. He, *ACS Appl. Mater. Interfaces* 2015, *7*, 250 – 255; c) M. Xuan, Z. Wu, J. Shao, L. Dai, T. Si, Q. He, *J. Am. Chem. Soc.* 2016, *138*, 6492 – 6497;

[23] d) Q. Rao, T. Si, Z. Wu, M. Xuan, Q. He, *Sci. Rep.* 2017, *7*, 4621. R. Dong, C. Wang, Q. Wang, A. Pei, X. She, Y. Zhang, Y. Cai, *Nanoscale* 2017, *9*, 15027 – 15032.

[24] M. Enachi, M. Guix, V. Postolache, V. Ciobanu, V. M. Fomin, O. G. Schmidt, I. Tiginyanu, *Small* 2016, *12*, 5497 – 5505.

[25] B. Jurado-S#nchez, J. Wang, A. Escarpa, *ACS Appl. Mater. Interfaces* 2016, *8*, 19618 – 19625.

[26] R. Maria-Hormigos, B. Jurado-Sanchez, L. Vazquez, A. Escarpa, *Chem. Mater.* 2016, *28*, 8962 – 8970.

[27] R. Narayanan, B. N. Reddy, M. Deepa, *J. Phys. Chem. C* 2012, *116*, 7189 – 7199.

[28] a) Y. L. Chan, S. Y. Pung, S. Sreekantan, F. Y. Yeoh, *J. Exp. Nanosci.* 2016, *11*, 603 – 618; b) T. Li, J. Wu, X. Xiao, B. Zhang, Z. Hu, J. Zhou, P. Yang, X. Chen, B. Wang, L. Huang, *RSC Adv.*

[29] 2016, *6*, 13914 – 13919. J. R. Harbour, J. Tromp, M. L. Hair, *Can. J. Chem.* 1985, *63*, 204 – 208.

[30] A. Jodra, F. Soto, M. A. Lopez-Ramirez, A. Escarpa, J. Wang, *Chem. Commun.* 2016, *52*, 11838 – 11841.

[31] c. Bjçrkbacka, M. Yang, C. Gasparrini, C. Leygraf, M. Jonsson, *Dalton Trans.* 2015, *44*, 16045 – 16051.

[32] L. H. Jin, C. S. Han, *Anal. Chem.* 2014, *86*, 7209 – 7213.

[33] C. Ratanatawanate, A. Bui, K. Vu, K. J. Balkus, *J. Phys. Chem. C* 2011, *115*, 6175 – 6180.

[34] Y. Z. Wang, A. M. Beccaria, G. Poggi, *Corros. Sci.* 1994, *36*, 1277 – 1288.